Article

Self-Assembly of Designed Oligomeric Siloxanes with Alkyl Chains into Silica-Based Hybrid Mesostructures

Atsushi Shimojima, Zheng Liu, Tetsu Ohsuna, Osamu Terasaki, and Kazuyuki Kuroda

J. Am. Chem. Soc., **2005**, 127 (40), 14108-14116• DOI: 10.1021/ja0541736 • Publication Date (Web): 21 September 2005

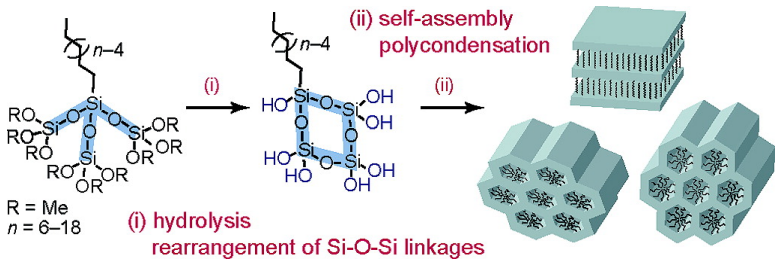

More About This Article

Additional resources and features associated with this article are available within the HTML version:

- Supporting Information
- Links to the 14 articles that cite this article, as of the time of this article download
- Access to high resolution figures
- Links to articles and content related to this article
- Copyright permission to reproduce figures and/or text from this article

View the Full Text HTML

J|A|C|S
ARTICLES
Published on Web 09/21/2005

Self-Assembly of Designed Oligomeric Siloxanes with Alkyl Chains into Silica-Based Hybrid Mesostructures

Atsushi Shimojima,*[,||,⊥] Zheng Liu,[‡,§] Tetsu Ohsuna,[§] Osamu Terasaki,[§] and Kazuyuki Kuroda*[,†,||,⊥]

Contribution from the Department of Applied Chemistry, Waseda University, Ohkubo-3, Shinjuku-ku, Tokyo 169-8555, Japan, Research Center for Advanced Carbon Materials, National Institute of Advanced Industrial Science and Technology (AIST), Tsukuba, Ibaraki 305-8565, Japan, Structural Chemistry, Arrhenius Laboratory, Stockholm University, S-10691 Stockholm, Sweden, Kagami Memorial Laboratory for Materials Science and Technology, Waseda University, Nishiwaseda-2, Shinjuku-ku, Tokyo 169-0051, Japan, and CREST, Japan Science and Technology Agency (JST), Japan

Received June 24, 2005; E-mail: a-shimo@kurenai.waseda.jp; kuroda@waseda.jp

Abstract: A novel self-assembly route to ordered silica−organic hybrids using well-defined siloxane oligomers with alkoxy functionality and covalently attached alkyl chains has been investigated. Various hybrid mesostructures were obtained by hydrolysis and polycondensation without the use of any structure-directing agents. The oligomers **1(C*n*)**, having an alkylsilane core and three branched trimethoxysilyl groups, formed highly ordered lamellar phases when $n = 14-18$, while those with shorter alkyl chains formed cylindrical assemblies, slightly distorted two-dimensional (2D) hexagonal structures ($n = 6-10$), and a novel 2D monoclinic structure ($n = 12$). Furthermore, the mixtures of **1(C*n*)** with different chain lengths yielded well-ordered 2D hexagonal phases, possibly due to the better packing of the precursors. The hybrids consisting of cylindrical assemblies were converted to ordered porous silica with tunable pore sizes upon calcination to remove organic groups. The liquid-state ^{29}Si NMR analysis of the hydrolysis and polycondensation processes of **1(C*n*)** revealed a unique intramolecular reaction yielding primarily the oligomer with a tetrasiloxane ring which is a new class of amphiphilic molecule having both self-assembling ability and high cross-linking ability. We also found that the mesostructure (lamellar or 2D hexagonal) was strictly controlled by varying the number of siloxane units per alkyl chain. These results provide a deeper understanding of the present self-assembly process that is strongly governed by the molecular packing of oligosiloxane precursors.

Introduction

The design of nanomaterials through self-assembly is one of the most exciting areas of research in nanoscience and nanotechnology. Recently, self-assembly of amphiphilic molecules[1] has been widely used for the production of inorganic−organic nanocomposites with controlled structures and morphologies. It is well-established that various mesostructured composites can be obtained by using surfactants as structure-directing agents.[1d,2] However, their formation process is complicated, relying on the weak interactions between surfactant and inorganic species. The molecular design of inorganic−organic hybrid precursors capable of self-assembly and subsequent inorganic cross-linking would provide a direct and efficient pathway to novel nanoarchitectures where each component is precisely arranged at the molecular scale. Although there have been a few reports on the use of precursors where surfactants are covalently attached to inorganic species,[3,4] the "surfactant-free" synthesis of hybrid mesostructures still remains a significant challenge for fundamental research.

Much attention is currently being paid to self-directed assembly during hydrolysis and polycondensation of organoalkoxysilane precursors with the general formula of $R'[-Si(OR)_3]_m$.[5] Such a method is expected to provide a new class of

† Department of Applied Chemistry, Waseda University.
‡ AIST.
§ Stockholm University.
|| Kagami Memorial Laboratory for Materials Science and Technology, Waseda University.
⊥ CREST, JST.

(1) (a) Ringsdorf, H.; Schlarb, B.; Venzmer, J. *Angew. Chem., Int. Ed. Engl.* **1988**, *27*, 113−158. (b) Tschierske, C. *J. Mater. Chem.* **1998**, *8*, 1485−1508. (c) Hyde, S. T.; Schröder, G. E. *Curr. Opin. Colloid Interface Sci.* **2003**, *8*, 5−14. (d) Förster, S.; Plantenberg, T. *Angew. Chem., Int. Ed.* **2002**, *41*, 688−714.
(2) (a) Ying, J. Y.; Mehnert, C. P.; Wong, M. S. *Angew. Chem., Int. Ed.* **1999**, *38*, 56−77. (b) Ozin, G. A. *Chem. Commun.* **2000**, 419−432. (c) Soler-Illia, G. J. d. A. A.; Sanchez, C.; Lebeau, B.; Patarin, J. *Chem. Rev.* **2002**, *102*, 4093−4138. (d) van Bommel, K. J. C.; Friggeri, A.; Shinkai, S. *Angew. Chem., Int. Ed.* **2003**, *42*, 980−999.
(3) (a) Antonelli, D. M.; Ying, J. Y. *Angew. Chem., Int. Ed. Engl.* **1995**, *34*, 2014−2017. (b) Antonelli, D. M.; Nakahira, A.; Ying, J. Y. *Inorg. Chem.* **1996**, *35*, 3126−3136.
(4) (a) Huo, Q.; Margolese, D. I.; Stucky, G. D. *Chem. Mater.* **1996**, *8*, 1147−1160. (b) Ruiz-Hitzky, E.; Letaïef, S.; Prévot, V. *Adv. Mater.* **2002**, *14*, 439−443. (c) Zhang, Q.; Ariga, K.; Okabe, A.; Aida, T. *J. Am. Chem. Soc.* **2004**, *126*, 988−989.
(5) (a) Boury, B.; Corriu, R. J. P. *Chem. Commun.* **2002**, 795−802. (b) Boury, B.; Corriu, R. *Chem. Rec.* **2003**, *3*, 120−132.

10.1021/ja0541736 CCC: $30.25

nanostructured silica-based hybrids that are not accessible by using surfactants as structure-directing agents,[6] or by post modification of mesoporous silica or layered silicates by silylation.[6a,7] Long-chain alkyltrialkoxysilanes were found to form hybrids with lamellar structures due to the amphiphilicity of the hydrolyzed monomers.[4a,8] Lamellar hybrids have also been prepared from bistrialkoxysilane precursors, $(RO)_3Si-R'-Si(OR)_3$, having rigid and/or self-associating organic groups.[9] Furthermore, synthetic peptide lipids and amphiphilic block copolymers bearing $-Si(OR)_3$ groups have been used to form vesicular assemblies.[10,11] However, the chemical design of organosilane precursors that allows for the control of mesostructures has been very limited. In particular, higher-curvature mesophases such as 2D hexagonal and cubic can be obtained only when both a hydrophobic chain and a cationic head are integrated in the organic group.[4] Corriu et al. recently reported the formation of a 2D hexagonal hybrid from bis(trimethoxysilyl)alkane with a long alkylene spacer; however, the structure is not yet well characterized due to the instability of the framework.[12]

To establish a new design concept, the incorporation of an oligomeric siloxane unit instead of a single $-Si(OR)_3$ group should be important because of the potential control over the molecular shape, hydrophobic−hydrophilic balance, and cross-linking ability of the molecules. We recently succeeded in synthesizing oligomeric precursors, tris(trimethoxysilyloxy)-alkylsilanes (**1(C*n*)**, $n = 10$ and 16), which can self-assemble into either lamellar ($n = 16$) or 2D hexagonal-like ($n = 10$) hybrids by hydrolysis and polycondensation.[13] The well-defined oligomeric siloxane unit as well as the alkyl chain length are crucial for the variation of mesostructures, because alkyltrialkoxysilanes ($C_nH_{2n+1}Si(OR)_3$, $n = 8-18$) exclusively form lamellar phases even by co-condensation with tetraalkoxysilanes.[14] Although siloxane- or carbosilane-based oligomers and dendrimers have been used as building blocks to construct nanomaterials with controlled microstructures,[15−17] their mesoscale organization has been attained only in the presence of surfactants.[18] Thus, the self-assembly of the precursors containing an oligosiloxane part acting as both a hydrophilic head and a cross-linking unit is very unique. However, until now, little is known about their detailed phase behavior and hydrolysis and polycondensation processes.

In this paper, we report the designed synthesis of mesostructured hybrids from a series of oligosiloxane precursors and discuss the molecular factor affecting the self-assembly process. In addition to the alkyl chain lengths (**1(C*n*)**, $n = 4$, 6, 8, 10, 12, 14, 16, and 18), we also examined the variation of the average number of siloxane units either by the addition of $Si(OR)_4$ during the reaction or by the use of an oligomeric precursor (**2**) containing only two $-Si(OR)_3$ groups. The structural characterization at molecular and mesoscopic scales was performed using X-ray diffraction (XRD), transmission electron microscopy (TEM), and solid-state NMR. Furthermore, the hydrolysis and polycondensation processes of such oligomeric precursors were investigated by liquid-state ^{29}Si NMR to elucidate the structure of intermediate species involved in the self-assembly.

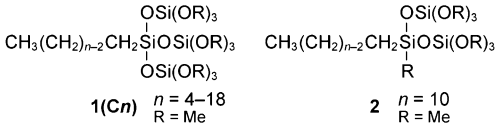

Experimental Section

Precursor Synthesis. Tris(trimethoxysilyloxy)(alkyl)silane ($C_nH_{2n+1}Si(OSi(OMe)_3)_3$, $n = 4$, 6, 8, 10, 12, 14, 16, and 18) (1(C*n*)). The synthesis was accomplished by silylation of alkylsilanetriols prepared by hydrolysis of alkyltrichlorosilanes ($n = 4-12$) or alkyltriethoxysilanes ($n = 14-16$) (see Supporting Information) with tetrachlorosilane ($SiCl_4$, Tokyo Kasei Kogyo Co., Ltd.), followed by methanolysis of Si−Cl groups. All reactions were performed under nitrogen atmosphere using standard Schlenk techniques. Typically, 12.0 g of alkylsilanetriols dissolved in dried tetrahydrofuran (THF, 600 mL) was added to a mixture of $SiCl_4$ (100 mL) and hexane (120 mL) with vigorous stirring at room temperature. The solvents and unreacted $SiCl_4$ were then removed in vacuo to afford slightly turbid liquids that contained mainly $RSi(OSiCl_3)_3$ (R = alkyl) and $RSiCl(OSiCl_3)_2$ (15−20%, evaluated by ^{29}Si NMR). From these mixtures, $RSi(OSiCl_3)_3$ was roughly isolated by vacuum distillation. The methanolysis of $RSi(OSiCl_3)_3$ was performed by either (1) addition of an excess of dried methanol with degassing of HCl under reduced pressure or (2) addition of methanol (excess) in the presence of hexane and pyridine. The former procedure was repeated several times to eliminate Si−Cl groups, while the latter required a subsequent filtration step to remove pyridine hydrochloride. The products were finally purified by vacuum distillation to yield **1(C*n*)** as clear and colorless liquids. Spectroscopic data are presented in the Supporting Information.

Bis(trimethoxysilyloxy)(decyl)(methyl)silane ($C_{10}H_{21}SiMe(OSi(OMe)_3)_2$) (2). Decylmethyldichlorosilane (Tokyo Kasei Kogyo Co., Ltd., 24.3 g) in diethyl ether (250 mL) was added dropwise to a vigorously stirred mixture of diethyl ether (250 mL), THF (400 mL), H_2O (3.8 mL), and aniline (19.1 mL) in an ice bath. After stirring for 1 h, the precipitates (aniline hydrochloride) were removed by filtration, and solvents were then completely evaporated under reduced pressure.

(6) For example, see (a) Stein, A.; Melde, B. J.; Schroden, R. C. *Adv. Mater.* **2000**, *12*, 1403−1419. (b) Sayari, A.; Hamoudi, S. *Chem. Mater.* **2001**, *13*, 3151−3168. (c) Lu, Y.; Fan, H.; Doke, N.; Loy, D. A.; Assink, R. A.; LaVan, D. A.; Brinker, C. J. *J. Am. Chem. Soc.* **2000**, *122*, 5258−5261. (d) Inagaki, S.; Guan, S.; Ohsuna, T.; Terasaki, O. *Nature* **2002**, *416*, 304−307.
(7) (a) Ogawa, M.; Okutomo, S.; Kuroda, K. *J. Am. Chem. Soc.* **1998**, *120*, 7361−7362. (b) Shimojima, A.; Mochizuki, D.; Kuroda, K. *Chem. Mater.* **2001**, *13*, 3603−3609.
(8) Shimojima, A.; Sugahara, Y.; Kuroda, K. *Bull. Chem. Soc. Jpn.* **1997**, *70*, 2847−2853.
(9) (a) Moreau, J. J. E.; Vellutini, L.; Man, M. W. C.; Bied, C.; Bantignies, J.-L.; Dieudonné, P.; Sauvajol, J.-L. *J. Am. Chem. Soc.* **2001**, *123*, 7957−7958. (b) Ben, F.; Boury, B.; Corriu, R. J. P. *Adv. Mater.* **2002**, *14*, 1081−1084. (c) Liu, N.; Yu, K.; Smarsly, B.; Dunphy, D. R.; Jiang, Y.-B.; Brinker, C. J. *J. Am. Chem. Soc.* **2002**, *124*, 14540−14541. (d) Moreau, J. J. E.; Pinchon, B. P.; Man, M. W. C.; Bied, C.; Pritzkow, H.; Bantignies, J.-L.; Dieudonné, P.; Sauvajol, J.-L. *Angew. Chem., Int. Ed.* **2004**, *43*, 203−206.
(10) (a) Katagiri, K.; Ariga, K.; Kikuchi, J. *Chem. Lett.* **1999**, 661−662. (b) Katagiri, K.; Hamasaki, R.; Ariga, K.; Kikuchi, J. *J. Am. Chem. Soc.* **2002**, *124*, 7892−7893.
(11) (a) Koh, K.; Ohno, K.; Tsujii, Y.; Fukuda, T. *Angew. Chem., Int. Ed.* **2003**, *42*, 4194−4197. (b) Du, J.; Chen, Y.; Zhang, Y.; Han, C. C.; Fischer, K.; Schmidt, M. *J. Am. Chem. Soc.* **2003**, *125*, 14710−14711.
(12) Alauzun, J.; Mehdi, A.; Reyé, C.; Corriu, R. J. P. *J. Mater. Chem.* **2005**, *15*, 841−843.
(13) Shimojima, A.; Kuroda, K. *Angew. Chem., Int. Ed.* **2003**, *42*, 4057−4060.
(14) Shimojima, A.; Kuroda, K. *Langmuir* **2002**, *18*, 1144−1149.
(15) Brinker, C. J.; Scherer, G. W. *Sol−Gel Science*; Academic Press: San Diego, CA, **1990**.
(16) (a) Klemperer, W. G.; Mainz, V. V.; Millar, D. M. *Mater. Res. Soc. Symp. Proc.* **1986**, *73*, 3−13. (b) Day, V. W.; Klemperer, W. G.; Mainz, V. V.; Millar, D. M. *J. Am. Chem. Soc.* **1985**, *107*, 8262−8264.
(17) (a) Lang, H.; Lühmann, B. *Adv. Mater.* **2001**, *13*, 1523−1540. (b) Kriesel, J. W.; Tilley, T. D. *Chem. Mater.* **1999**, *11*, 1190−1193. (c) Boury, B.; Corriu, R. J. P.; Nuñez, R. *Chem. Mater.* **1998**, *10*, 1795−1804.
(18) (a) Fyfe, C. A.; Fu, G. *J. Am. Chem. Soc.* **1995**, *117*, 9709−9714. (b) Firouzi, A.; Atef, F.; Oertli, A. G.; Stucky, G. D.; Chmelka, B. F. *J. Am. Chem. Soc.* **1997**, *119*, 3596−3610. (b) Landskron, K.; Ozin, G. A. *Science* **2004**, *306*, 1529−1532.

The solid residue, mainly consisting of decylmethylsilanediol, was all dissolved in dried THF (500 mL) and added to the mixture of $SiCl_4$ (75 mL) and hexane (200 mL) under nitrogen atmosphere. After the removal of volatile components in vacuo, methanolysis of the siloxane species was conducted in a similar manner as for **1(C*n*)**. Vacuum distillation of the oily residue gave **2** as a clear and colorless liquid. ^{1}H NMR (500 MHz, $CDCl_3$): δ (ppm) 0.20 (s, 3H; $SiCH_3$), 0.64−0.67 (m, 2H), 0.87−0.89 (t, 3H; CH_3), 1.27 (m, 12H), 1.30−1.34 (m, 2H), 1.39−1.44 (m, 2H), 3.57 (s, 18H; OCH_3); ^{13}C NMR (125.7 MHz, $CDCl_3$): δ (ppm) −1.17, 14.14, 16.83, 22.67, 22.81, 29.46, 29.49, 29.69, 29.79, 32.06, 33.30, and 51.04; ^{29}Si NMR (99.3 MHz, $CDCl_3$): δ (ppm) −85.51 (Q^1), −18.04 (D^2).

Synthesis of Silica-Based Hybrids. Hydrolysis and polycondensation reactions of the precursors (**1(C*n*)** and **2**) were performed in solution with molar ratios of **1(C*n*)**/THF/H_2O/HCl = 1:50:18:0.002 and **2**/THF/H_2O/HCl = 1:50:12:0.002, respectively. The mixtures were stirred at 25 °C for 12 h, and water (H_2O/**1(C*n*)** = 32, H_2O/**2** = 38, respectively) was then added. We note that the additional water ensures the homogeneity of the films in the cases of $n \geq 14$ and appears to have no effect on the nanostructures of the resulting hybrids. The precursor solutions were cast on glass substrates (∼0.03 mL cm^{-2}) and air-dried at room temperature for 2 days to promote polycondensation. The resulting thick films (15−20 μm in thickness) were scraped off from the substrate and pulverized before characterization. Thin films (450−600 nm in thickness) were also prepared by spin-coating (3000 rpm, 10 s) the precursor solutions on glass substrates (Corning #7059) in air at a relative humidity of 35−45%. Furthermore, the incorporation of an additional silica source was performed by adding TMOS and H_2O (TMOS/**1(C*n*)** = 1, H_2O/TMOS = 4) to the precursor solution of **1(C*n*)** (n = 14, 16, and 18) after 12 h of reaction, and the mixtures were stirred for another 2 h before casting on glass substrate.

Characterization. The XRD patterns of the products were obtained on a Mac Science M03XHF22 diffractometer with Mn-filtered Fe Kα radiation. TEM studies were carried out on JEOL JEM-2010, JEM-3010, and JEM-4000EX microscopes operated at 200, 300, and 400 kV, respectively. To prepare TEM samples, powders were ground with mortar and pestle and dispersed in ethanol. A carbon-coated copper grid was immersed in this dispersion and allowed to dry in air. Solid-state ^{13}C CP/MAS NMR spectra were recorded on a JEOL JNM-CMX-400 spectrometer at a resonance frequency of 100.53 MHz with a contact time of 2 ms and a recycle delay of 5 s. Samples were put into 7.5-mm (or 5-mm) zirconia rotors and spun at 5 kHz. Liquid-state ^{29}Si NMR spectra of the precursor solutions were recorded on a JEOL Lambda-500 spectrometer at a resonance frequency of 99.05 MHz with a pulse width of 6.5 μs, and 64 scans were acquired with a recycle delay of 10 s. The solutions were put in a 5-mm glass tube, where THF-d_8 was used for obtaining lock signals, and a small amount of chromium(III) acetylacetonate was added for the relaxation of ^{29}Si nuclei. Chemical shifts for both ^{29}Si and ^{13}C NMR were referenced to tetramethylsilane at 0 ppm. Nitrogen adsorption measurements were performed by an Autosorb-1 instrument (Quantachrome Instruments, Inc) at 77 K. Samples were preheated at 120 °C for 3 h under 1 × 10^{-2} Torr. The Brunauer−Emmett−Teller (BET) surface area was calculated from the adsorption data in the relative pressure range from 0.02 to 0.05. The pore size distribution was evaluated using the nonlocal density functional theory (NLDFT).[19]

Results and Discussion

Structures of Silica-Based Hybrids Derived from 1(C*n*). Thick films obtained by casting the precursor solution on glass substrates showed birefringence due to the structural ordering when $n \geq 6$. The XRD patterns of the powdered samples derived from **1(C*n*)** with various alkyl chain lengths are shown in Figure 1. The patterns for n = 14, 16, and 18 show the strongest diffraction peaks at small scattering angle (d = 3.05, 3.38, and 3.59 nm, respectively) and their higher-order reflections up to the fifth order, indicating the lamellar structures of these samples. On the other hand, the XRD patterns of the hybrids with shorter alkyl chains (n = 6, 8, 10, and 12) are quite different, showing the strongest peaks at d = 2.13, 2.52, 2.92, and 3.35 nm, respectively. The relationship between the d value and alkyl chain length is linear, but differs from that for the lamellar hybrids with $n \geq 14$ (inset of Figure 1). The hybrids with n = 8 and 10 exhibit three main peaks, characteristic of a 2D hexagonal mesostructure (10, 11, and 20 reflections). However, each (10) peak has a slight shoulder at smaller 2θ angle (see Supporting Information, Figure S1, where the intensities are plotted on a logarithmic scale), which might be due to the distortion of the structure from an ideal 2D hexagonal lattice. The pattern for n = 6 also shows a sharp peak with a small shoulder, though the peaks at higher angle are less-defined. When the chain length decreased to n = 4, only a weak and broad peak (d = ∼1.9 nm) was observed, suggesting the low self-assembling ability of this precursor. Remarkably, the hybrid with n = 12 shows a well-defined pattern exhibiting a shoulder peak and three additional peaks at d = 2.40, 1.86, and 1.68 nm, and these peaks are not assigned to the 2D hexagonal structure.

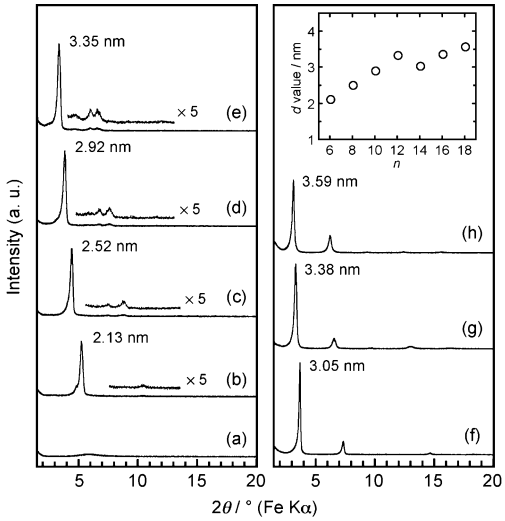

Figure 1. Powder XRD patterns of the hybrids (as-synthesized) derived from **1(C*n*)**: (a) n = 4, (b) n = 6, (c) n = 8, (d) n = 10, (e) n =12, (f) n = 14, (g) n = 16, and (h) n = 18. The inset shows the variation in the d value as a function of the alkyl chain length n.

The nanostructures of these hybrids were further studied by TEM. In contrast to the lamellar hybrids (n = 14−18) showing only striped patterns, the TEM images of the hybrids with n = 6−12 revealed that they consisted of arrays of cylindrical assemblies. The hybrids with n = 6, 8, and 10 show typical images of 2D hexagonal mesostructures, where both hexagonally ordered patterns (Figure 2) and striped patterns are observable, depending on the direction of electron incidence either parallel or perpendicular to the channel. However, it appears that the structures are slightly distorted. As expected from the XRD data, a unique structure was observed for n = 12. The high-resolution images (Figure 3) reveal an ordered arrangement of distorted hexagonal rods, and the structure is far from being 2D hexagonal.

(19) Ravikovitch, P. I.; Wei, D.; Chueh, W. T.; Haller, G. L.; Neimark, A. V. *J. Phys. Chem. B* **1997**, *101*, 3671−3679.

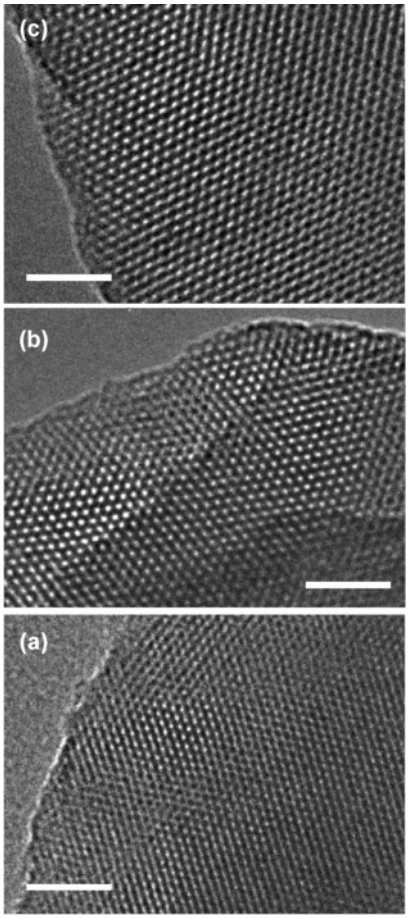

Figure 2. Typical TEM images of the hybrids (as-synthesized) derived from **1(C*n*)**: (a) $n = 6$, (b) $n = 8$, (c) $n = 10$. Scale bar, 20 nm. They were taken by a JEM-2010 microscope.

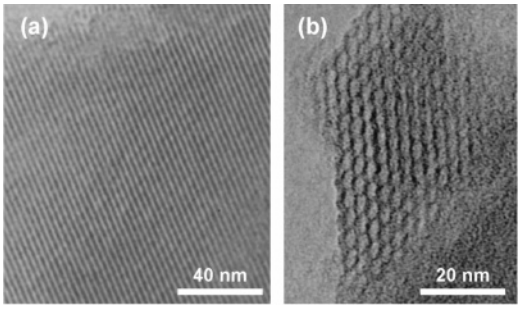

Figure 3. TEM images of the hybrids (as-synthesized) derived from **1-(C12)**. Views (a) perpendicular and (b) parallel to the long axis of the cylindrical assembly. They were taken by a JEM-4000EX microscope.

A distortion of 2D hexagonal structure along the [10] direction is often observed for thin films of mesostructured silica due to the anisotropic shrinkage of siloxane networks.[20] Some anisotropic shrinkage could also occur in our system because the hybrids were obtained as thick films on glass substrates. However, the structure shown in Figure 3b is not simply derived from the 2D hexagonal structure by distorting along the [10] direction, and it was observed throughout the sample. It is also noted that the degree of distortion is dependent on the alkyl chain length ($n = 6-12$), and well-ordered 2D hexagonal phases can be obtained from the mixtures of two precursors with

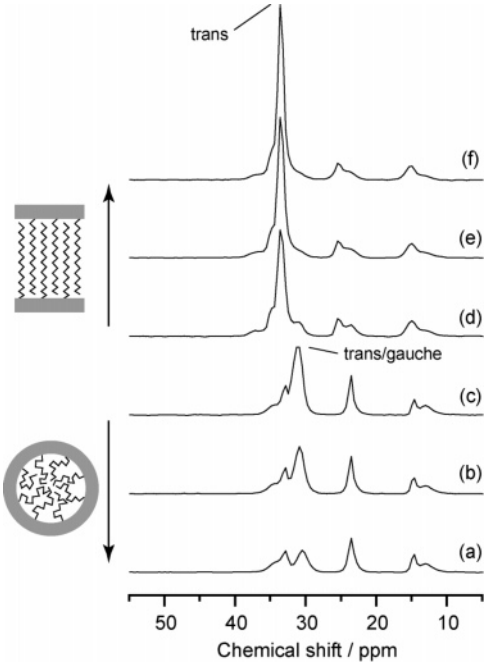

Figure 4. ^{13}C CP/MAS NMR spectra (as-synthesized) derived from **1-(C*n*)**: (a) $n = 8$, (b) $n = 10$, (c) $n = 12$, (d) $n = 14$, (e) $n = 16$, (f) $n = 18$. The inset shows the schematic illustrations of alkyl chains in the cylindrical and lamellar assemblies.

different chain length, as described later. We therefore consider that the structure for $n = 12$ is associated with the molecular packing of alkylsiloxane units and is possibly an intermediate phase between lamellar and 2D hexagonal. Such a behavior is inherent to the present system. The surfactant/silicate systems generally afford highly symmetrical structures except for the report by Zhao et al.,[21] who discovered a 2D mesostructure with a centered rectangular lattice (SBA-8) using rigid bolaform surfactants.

The variation of the mesostructure (cylindrical or lamellar) is accompanied by the conformational change of the alkyl chains, as evidenced by the chemical shifts of the interior methylene carbons in the ^{13}C CP/MAS NMR spectra (Figure 4). The spectra for $n = 14-18$ show the signals at 33.7 ppm indicative of all-trans chains, whereas in the cases of $n = 8-12$ the signals are shifted to 30.6−31.2 ppm due to those with mixed trans-gauche conformations.[22] The lamellar hybrids ($n = 14-18$) have highly ordered interlayer chains as compared to the lamellar hybrids derived from alkyltriethoxysilane/tetraethoxysilane systems[14] which contained the chains with the trans-gauche conformation. The alkyl chains appear to be arranged in an interdigitated monolayer fashion, because the d values and the average increment of the d value per CH_2 group ($\Delta d/CH_2 = \sim 0.13$ nm) are much smaller than those for the lamellar alkylsiloxanes with bilayer arrangements of all-trans chains ($d = 4.28$, 4.80, and 5.28 nm ($\Delta d/CH_2 = 0.25$)).[8] The $\Delta d/CH_2$ value of ∼0.13 indicates that alkyl chains are aligned almost perpendicularly to the siloxane layers.

The average thickness of the siloxane layer of the lamellar hybrids is roughly estimated to be 1.2 nm by extrapolating the plot ($n = 14-18$ in the inset of Figure 1) to $n = 0$. For the

(20) Klotz, M.; Albouy, P.-A.; Ayral, A.; Ménager, C.; Grosso, D.; Van der Lee, A.; Cabuil, V.; Babonneau, F.; Guizard, C. *Chem. Mater.* **2000**, *12*, 1721−1728.

(21) Zhao, D.; Huo, Q.; Feng, J.; Kim, J.; Han, Y.; Stucky, G. D. *Chem. Mater.* **1999**, *11*, 2668−2672.

(22) Wang, L.-Q.; Exarhos, G. J.; Liu, J. In *Characterization of Nanophase Materials*; Wang, Z. L., Ed.; Wiley-VCH: Weinheim, 2000; pp 243−260.

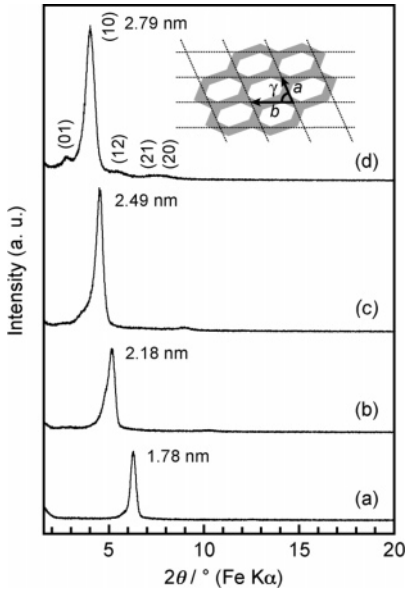

Figure 5. Powder XRD patterns of the hybrids derived from **1(C*n*)** after calcination at 500 °C for 8 h: (a) $n = 6$, (b) $n = 8$, (c) $n = 10$, (d) $n = 12$.

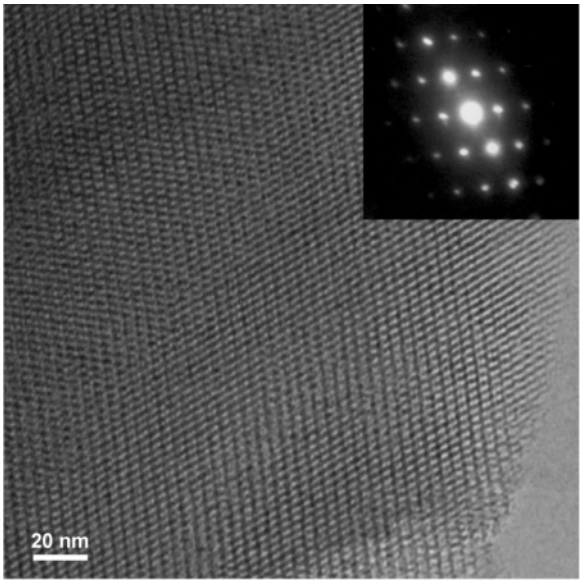

Figure 6. TEM image and ED pattern (inset) of the hybrid derived from **1(C12)** after calcination at 500 °C for 8 h. They were taken by a JEM-3010 microscope.

Table 1. Structural Parameters of the Calcined Samples Derived from **1(C*n*)** Evaluated from Nitrogen Adsorption Data

n	BET surface area ($m^2\ g^{-1}$)	pore volume ($cm^3\ g^{-1}$)	NLDFT pore diameter (nm)
6	510	0.22	1.1
8	840	0.34	1.7
10	950	0.43	2.2
12	800	0.46	2.7

hybrids with $n = 6-12$, the thickness of the siloxane layers is calculated to be ~1.0 nm (0.9 nm ($n = 0$) × $2/\sqrt{3}$), when assuming a 2D hexagonal structure. Even though there are some errors due to the insufficient number of plots, these values suggest that the siloxane frameworks consist of bilayers of oligosiloxane units derived from **1(C*n*)**.

It is noteworthy that the lamellar hybrids have the ability to adsorb alkyl alcohols within their expandable interlayer spaces. Large increases of the *d*-spacings (Δd = ca. 1.3 nm) were observed when the samples were immersed in liquid decyl alcohol (Supporting Information, Figure S2). The hydrophobic interaction with interlayer alkyl chains and the hydrogen bonding with surface silanol groups should be essential for this adsorption property, as reported for alkylsilylated derivatives of crystalline layered silicates (e.g., kanemite and magadiite).[7]

Conversion to Porous Silica by Calcination. The hybrids with $n = 6-12$ can be used to produce ordered porous silica by calcination in air at 500 °C for 8 h to remove organic components. The XRD patterns of the calcined samples are shown in Figure 5. All the samples retain the ordered mesostructures, though the *d*-spacings are smaller by about 0.3−0.5 nm than those before calcination. The patterns for $n = 6$, 8, and 10 (Figure 5, parts a−c) exhibit the strongest peaks at $d =$ 1.78, 2.18, and 2.49 nm and ill-defined peaks at higher 2θ angles. When $n = 12$ (Figure 5d), several peaks are clearly observed at both sides of the strongest peak ($d = 2.79$ nm). The TEM image and the corresponding electron diffraction (ED) pattern (Figure 6) reveal a monoclinic lattice, similar to that before calcination. The ED pattern was unchanged by varying the tilt angle of the sample, confirming the absence of a three-dimensional (3D) ordering. On the basis of these TEM results, all of the XRD peaks are assigned to a 2D monoclinic structure with $a = 3.05$ nm, $b = 4.58$ nm, and $\gamma = 66°$ (inset of Figure 5d).

The nitrogen adsorption isotherms of calcined samples displayed type I ($n = 6$ and 8) or type IV ($n = 10$ and 12) curves typical of microporous and mesoporous silica, respectively (Supporting Information, Figure S3). The structural parameters, including the BET surface areas, pore volumes, and average pore diameters evaluated by the NLDFT method, are listed in Table 1. Note that the pore diameters are larger than those calculated by the Barrett−Joyner−Halenda (BJH) method[23] (1.0, 1.4, and 1.7 nm for $n = 8$, 10, and 12, respectively). This is in agreement with the report that the BJH method underestimates the pore size of mesoporous silica (MCM-41).[19]

Although there are several reports on the use of alkyltrialkoxysilanes as templates for producing porous silica,[24] this is the first synthesis of well-ordered cylindrical pores. The BET surface areas and pore volumes are comparable to those of mesoporous silica prepared by using alkyltrimethylammonium surfactants.[2] Moreover, by varying the alkyl chain length, the pore size can be controlled in the range of micropore to mesopore, which is usually difficult to access by the surfactant-directed approach.[25] The self-assembling ability of **1(C*n*)** with relatively short alkyl chains and the absence of organic headgroups (i.e., the covalent bond between alkyl chains and siloxane units) should contribute to the creation of well-controlled small pores. It is of particular importance that an ordered structure was formed even from **1(C6)**, because the surfactants with C6 chains are generally not suitable for use as structure-directing agents.[26] Although the structural ordering

(23) Barrett, E. P.; Joyner, L. G.; Halenda, P. P. *J. Am. Chem. Soc.* **1951**, *73*, 373−380.
(24) (a) Park, M.; Komarneni, S.; Lim, W. T.; Heo, N. H.; Choi, J. *J. Mater. Res.* **2000**, *15*, 1437−1440. (b) Büchel, G.; Unger, K. K.; Matsumoto, A.; Tsutsumi, K. *Adv. Mater.* **1998**, *10*, 1036−1038.
(25) Ryoo, R.; Park, I.; Jun, S.; Lee, C. W.; Kruk, M.; Jaroniec, M. *J. Am. Chem. Soc.* **2001**, *123*, 1650−1657, and references therein.
(26) Beck, J. S.; Vartuli, J. C.; Kennedy, G. J.; Kresge, C. T.; Roth, W. J.; Schramm, S. E. *Chem. Mater.* **1994**, *6*, 1816−1821.

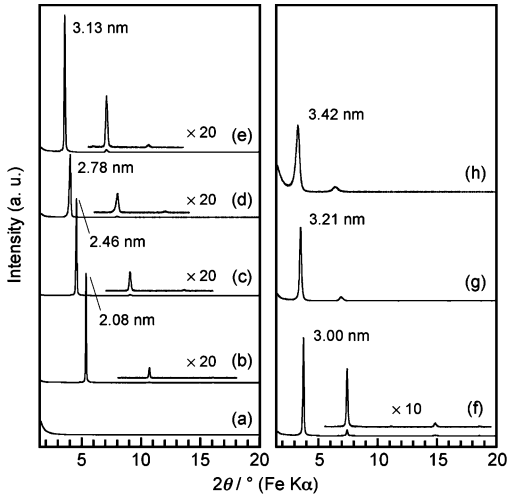

Figure 7. XRD patterns of the hybrids films (as-synthesized) derived from **1(C*n*)**: (a) $n = 4$, (b) $n = 6$, (c) $n = 8$, (d) $n = 10$, (e) $n = 12$, (f) $n = 14$, (g) $n = 16$, and (h) $n = 18$.

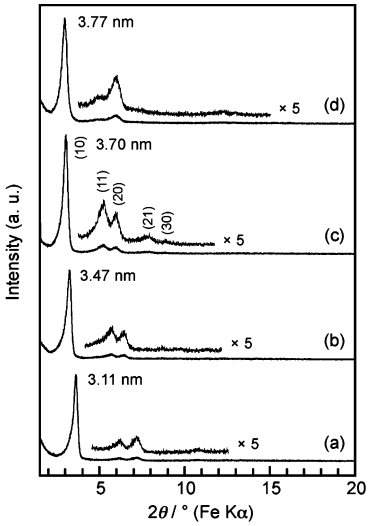

Figure 8. Powder XRD patterns of the as-synthesized hybrids derived from the 1:1 mixtures of (a) **1(C8)/1(C12)**, (b) **1(C10)/1(C14)**, (c) **1(C10)/1(C16)**, and (d) **1(C12)/1(C18)**.

decreased to some extent by calcination, to the best of our knowledge, the calcined sample derived from **1(C6)** possesses one of the smallest cylindrical pores that has ever been reported.

Film Formation. The thin films of the hybrids obtained by spin-coating were transparent and homogeneous, which is attributable to the high cross-linking ability of **1(C*n*)** containing three $-Si(OR)_3$ groups. The XRD patterns of the films are shown in Figure 7. The patterns for $n = 14-18$ are similar to those of the powdered samples, and are attributed to lamellar structures. The scanning electron microscopy (SEM) images of the cracked section of these films show undulating morphologies (Supporting Information, Figure S4), suggesting the incomplete orientation of the layers. On the other hand, the films for $n = 6-12$ have relatively flat and featureless cross-sections; they show sharp and intense XRD peaks with second- and third-order reflections. Such patterns are typical for a well-ordered 2D hexagonal structure with its long axis aligned parallel to the substrate surface,[27] as we confirmed for the **1(C10)**-derived film by cross-sectional TEM.[13] Unfortunately, the structural ordering of the films decreased significantly upon calcination at 500 °C for 8 h. For example, the XRD pattern of the calcined film derived from **1(C10)** shows a small, broad peak at $d = 1.6$ nm (data not shown).

Binary Systems of 1(C*n*) with Different Alkyl Chain Lengths. We have explored the possibility of controlling mesostructures by mixing two precursors with different alkyl chain lengths. Interestingly, a well-ordered 2D hexagonal phase was obtained from the 1:1 molar ratio of **1(C10)** and **1(C16)**. The XRD pattern of the as-synthesized hybrid (Figure 8c) displays five peaks indexed to the 10, 11, 20, 21, and 30 reflections associated with a 2D hexagonal symmetry ($d_{10} = 3.70$ nm). A well-ordered hexagonal structure was observed by TEM (Supporting Information, Figure S5). The d_{10} spacing is about 0.8 nm larger than that of the hybrids derived from **1-(C10)** and is even larger than the interlayer spacing of the lamellar hybrid derived from **1(C16)**. The ^{13}C CP/MAS NMR spectrum of this hybrid revealed the mixed trans-gauche conformation of alkyl chains (Supporting Information, Figure S6). These results indicate that both precursors are homogeneously distributed at the molecular level to form a new phase. It appears that the periodicity of the mesostructure can be adjusted in a certain range by varying the molar ratio of the precursors. For example, increasing the **1(C10)**/**1(C16)** ratio to 3:1 led to the formation of a 2D hexagonal structure with a smaller d_{10} value of 3.38 nm.

Furthermore, various combinations of precursors formed 2D hexagonal structures, except that the mixtures of long chain precursors ($14 \leq n$) yielded lamellar phases. The 1:1 mixtures of **1(C8)**/**1(C12)** and **1(C10)**/**1(C14)** formed 2D hexagonal phases with $d_{10} = 3.11$ and 3.47 nm, respectively (Figure 8a,b). Importantly, their XRD patterns are well-resolved compared to those obtained from the single precursors with intermediate chain lengths, that is, $n = 10$ and 12, respectively (Figure 1d,e), suggesting the better packing of the mixed alkyl chains to form circular cylinders. However, the **1(C12)/1(C18)** mixture resulted in a less-resolved XRD pattern where the (11) peak is relatively weak (Figure 8d). This is attributed to the strong interaction between C18 chains to induce inhomogeneity in the solid, as suggested by the ^{13}C CP/MAS NMR spectrum showing the presence of both all-trans and mixed trans-gauche domains (Supporting Information, Figure S6).

In all of the above systems, the mesostructures were retained after calcination (Supporting Information, Figure S7). While the XRD peaks became broad and weak in the case of the **1(C12)/1(C18)** system, other systems clearly show three peaks due to the 10, 11, and 20 reflections. The mesoporosities of these samples were confirmed by nitrogen adsorption analysis (Supporting Information, Figure S8). The BET surface areas, the average pore diameters (evaluated by the NLDFT method), and pore volumes are listed in Table 2. The pore diameter increases with increasing average chain length of two precursors. The relatively low BET surface area and pore volume for the **1-(C12)/1(C18)** system suggest the partial collapse of the mesostructure upon calcination.

Hydrolysis and Polycondensation Processes. To investigate the initial formation process of these hybrids, the reaction of

(27) (a) Yang, H.; Kuperman, A.; Coombs, N.; Mamiche-Afara, S.; Ozin, G. A. *Nature* **1996**, *379*, 703−705. (b) Hillhouse, H. W.; van Egmond, J. W.; Tsapatsis, M.; Hanson, J. C.; Larese, J. Z. *Microporous Mesoporous Mater.* **2001**, *44*−*45*, 639−643. (c) Alberius, P. C. A.; Frindell, K. L.; Hayward, R. C.; Kramer, E. J.; Stucky, G. D.; Chmelka, B. F. *Chem. Mater.* **2002**, *14*, 3284−3294.

Table 2. Structural Parameters of the Calcined Samples Derived from the 1:1 Mixtures of **1(C*n*)** Evaluated from Nitrogen Adsorption Data

samples	BET surface area ($m^2\ g^{-1}$)	pore volume ($cm^3\ g^{-1}$)	NLDFT pore diameter[a] (nm)
1(C8)/1(C12)	880	0.46	2.3
1(C10)/1(C14)	840	0.51	2.8
1(C10)/1(C16)	830	0.58	3.2
1(C12)/1(C18)	690	0.49	3.3

[a] For comparison: the BJH pore diameters are 1.4, 1.8, 2.1, and 2.2 nm for **1(C8)/1(C12)**, **1(C10)/1(C14)**, **1(C10)/1(C16)**, and **1(C12)/1(C18)** systems, respectively.

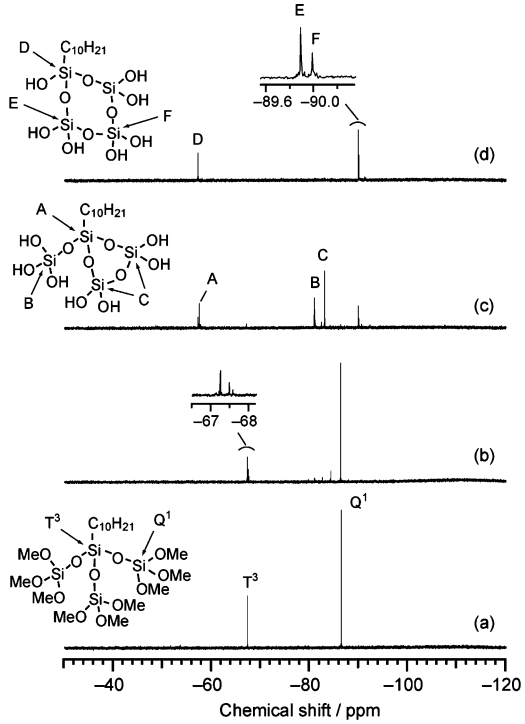

Figure 9. Liquid-state ^{29}Si NMR spectra of (a) **1(C10)** in THF, and the solutions after (b) 0.5 h, (c) 3 h, and (d) 12 h of reaction in the **1(C10)**/THF (10% THF-d_8)/H_2O/HCl = 1:50:18:0.002 system.

1(C10) in the solution was monitored by liquid-state ^{29}Si NMR. As shown in Figure 9a, the spectrum for **1(C10)** exhibits two signals at −67.3 and −86.4 ppm with the intensity ratio of 1:3. These signals are assigned to the T^3 (T^x, C*Si*$(OSi)_x(OH)_{3-x}$) and Q^1 (Q^x, *Si*$(OSi)_x(OH)_{4-x}$) units, originating from the alkylsiloxane unit and branched $-Si(OMe)_3$ groups, respectively.

As the reaction proceeds (Figure 9b), several signals due to the hydrolyzed $-Si(OMe)_3$ groups appear downfield in the Q^1 region, accompanying the slight shifts of the T^3 signal. Subsequently, three signals (labeled with A, B, and C) appear, and the unreacted precursor almost disappears after ∼3 h (Figure 9c). No signals of Q^0 species (from −71 to −79 ppm) were observed during the reaction, suggesting the very slow rate of hydrolysis of the Si−O−Si bonds in **1(C10)**. After 12 h (Figure 9d), a T^2 signal at −57.1 ppm and two close Q^2 signals at −89.9 and −90.0 ppm are dominant (labeled with D, E, and F, respectively). The intensity ratio of these signals is 1:2:1, being consistent with the *T*/*Q* ratio of 1:3 for the precursor **1(C10)**. Similar results were also obtained using **1(C6)** and **1(C16)**, independent of the alkyl chain length.

Trimethylsilylation of the alkylsiloxane species formed after 12 h of reaction was carried out to elucidate their structures by mass spectrometry. The ^{29}Si NMR spectrum of the silylated derivatives mainly showed the T^3 (−66.9 ppm) and Q^4 (−107.9 and −108.1 ppm) signals with the intensity ratio of 1:2:1, along with the several M^1 signals due to the trimethylsilyl groups (Supporting Information, Figure S9), indicating that the original siloxane structure was retained during silylation. The FAB-MS spectrum of this sample exhibits fragment peaks ([M^+-Me] and [M^+-$SiMe_3$]) due to the cyclic tetrameric unit with seven trimethylsilylated silanol groups (Supporting Information, Figure S10). These results indicate that the cyclic oligomer composed of three Q^2 units and one T^2 unit (inset of Figure 9d) is the predominant species in the solution after 12 h of the reaction. The quantitative analysis based on the internal standard (hexamethyldisilane) revealed that about 50−60% of **1(C10)** transformed into the cyclic tetrasiloxane species. Although other species should coexist in the solution, the formation of well-defined oligomeric species in such a high ratio is a very specific phenomenon that cannot be attained when starting from the mixture of alkyltrialkoxysilane and tetraalkoxysilane.[28]

The rearrangement of the branched structure of **1(C*n*)** into the tetrasiloxane ring is triggered by the intramolecular condensation between two branched Q^1 units to form a trisiloxane ring. Such an intramolecular reaction is plausible because cyclization of linear trimeric species was reported to be fast and to compete with intermolecular condensation.[29] Actually, the presence of the intermediate species with a trisiloxane ring is evidenced by the appearance of three ^{29}Si signals (A−C) in Figure 9c. The intensities of these signals decrease with increases in the signals of the cyclic tetrasiloxane species, while keeping a constant ratio of 1:1:2. Signals A and C can be assigned to the T^3 and Q^2 units of a trisiloxane ring, and signal B represents the branched Q^1 unit attached to the T^3 unit (inset of Figure 9c). These assignments are consistent with the general findings that the T^3 and Q^2 signals due to cyclic trisiloxanes appear close to the T^2 and Q^1 signals of branched (or linear) oligomers, respectively.[30,31] The presence of a trisiloxane ring was further supported by the significant downfield shifts of the T^3 and Q^4 signals in the ^{29}Si NMR spectrum of the trimethylsilylated species (Supporting Information, Figure S9). The tetrasiloxane ring can be formed by the cleavage of the trisiloxane ring to form a linear tetrameric species ($Q^1-T^2-Q^2-Q^1$) and subsequent intramolecular condensation between terminal Q^1 units.

In contrast to the lability of a strained trisiloxane ring, a tetrasiloxane ring is known to be thermodynamically stable.[31] In the present system, no change was observed in the ^{29}Si NMR spectrum shown in Figure 9d, even after the addition of water (H_2O/**1(C10)** = 32), and the oligomer with a tetrasiloxane ring was detectable over 1 day after the reaction. This indicates that the tetrasiloxane ring is relatively stable against cleavage and that the intermolecular condensation is very slow, probably due to the steric repulsion between covalently attached long alkyl chains.

The formation of cyclic oligomers from **1(C*n*)** is of great interest because cyclic siloxane units play an important role in the nucleation of zeolites and are present as building units in

(28) (a) Rodríguez, S. A.; Colón, L. A. *Chem. Mater.* **1999**, *11*, 754−762. (b) Shimojima, A.; Umeda, N.; Kuroda, K. *Chem. Mater.* **2001**, *13*, 3610−3616.
(29) Sanchez, J.; McCormick, A. V. *J. Non-Cryst. Solids* **1994**, *167*, 289−294.
(30) Feher, F. J.; Newman, D. A.; Walzer, J. F. *J. Am. Chem. Soc.* **1989**, *111*, 1741−1748.
(31) Damrau, U.; Marsmann, H. C. *J. Non-Cryst. Solids* **1994**, *168*, 42−48.

their frameworks. Recently, several reports have suggested that cyclic tetrasiloxane species are suitable building units for the self-assembly of silica−surfactant composite mesophases.[32] By using IR spectroscopy, the presence of tetrasiloxane rings is generally revealed by a weak and broad IR band at around 600 cm^{-1}.[32b] This band can be observed in the FT-IR spectrum of the hybrid derived from **1(C10)**, confirming the presence of residual tetrasiloxane rings in the siloxane networks (Supporting Information, Figure S11). However, we have not obtained evidence of structural ordering in the siloxane networks of the hybrids.

We reported that the solid-state ^{29}Si MAS NMR spectra of the hybrids with $n = 10$ and 16 showed signals corresponding to the T^1, T^2, and T^3 units and the Q^2, Q^3, and Q^4 units.[13] Despite the difference in the mesostructures with alkyl chain length, there was no large difference in the local structures of the siloxane frameworks. The presence of the T^2 units is consistent with the above results that the hybrids are mainly assembled from the cyclic tetrasiloxanes, though the small T^1 signal indicates further cleavage of siloxane bonds during the synthesis. The degree of condensation for the *T* units ($n = 10$) is calculated to be 81% (Supporting Information, Figure S12 and Table S1). For comparison, the value for the lamellar hybrid prepared from the 1:3 mixture of decyltrimethoxysilane (C10TMS) and tetramethoxysilane (TMOS) under the identical conditions is 64%. Thus, the use of the oligomeric precursor (**1(C*n*)**) overcame the problem of low co-condensation rate of the *T* and *Q* units, which should be responsible for the formation of the higher-curvature mesophase.

Effect of Molecular Structure on Self-Assembly. The hydrolyzed species of **1(C*n*)** are the polyhydroxy amphiphiles containing a hydrophobic alkyl chain and hydrophilic silanol groups. The oligomer with a tetrasiloxane ring is structurally somewhat similar to sugar-based surfactants such as alkylglycosides, which are reported to form liquid crystalline phases,[33] in terms of having ring structures bearing OH groups. The emergence of birefringence indicative of the transformation from the isotropic phase to anisotropic solids during the drying process was observed by cross-polarized microscopy.

The self-assembled structures of amphiphilic molecules are generally explained by a geometrical packing parameter $g = V/a_o l$, where *V* is the effective volume of the hydrophobic chain, a_o is the effective area of the headgroup, and *l* is the hydrophobic chain length.[6a,34] Self-assembly of hydrolyzed alkyltrialkoxysilanes, having a single $Si(OH)_3$ group, leads to lamellar phases exclusively.[8] Thus the formation of higher-curvature phases from **1(C*n*)** ($n = 6-12$) is attributed to the larger headgroup area of the oligosiloxane unit that reduces the *g* value. It is intriguing that the structure of hybrids strictly changes to lamellar when the alkyl chain length increases from $n = 12$ ($n = 13$)[35] to $n = 14$, because the variation of *n* does not cause a substantial change of the *g* value.[4a] We suppose that the stronger hydrophobic interaction between longer alkyl chains favors the formation of all-trans lamellar assembly,[36] where interdigitated arrangements of alkyl chains compensate for the intermolecular space resulted from the large headgroup. The formation of 2D hexagonal phases upon addition of short chain precursors is attributed to the decrease in the effective volume of hydrophobic chains, in combination with the difficulty in the close packing of mixed long and short alkyl chains.

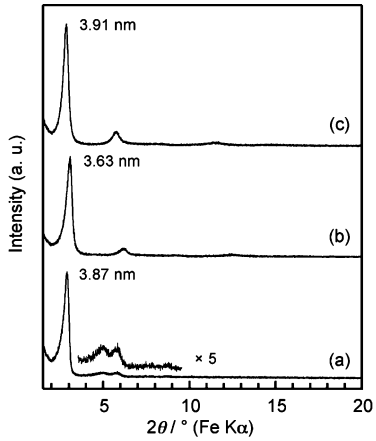

Figure 10. Powder XRD patterns of the as-synthesized hybrids prepared with the molar ratio of TMOS/**1(C*n*)** = 1: (a) $n = 14$, (b) $n = 16$, (c) $n = 18$.

The control of the mesostructure is also achieved by modifying the effective area of siloxane headgroups. The increase of the average number of SiO_4 (or $CSiO_3$) units per alkyl chain was performed by adding TMOS (TMOS/**1(C*n*)** = 1) into the precursor solutions of **1(C*n*)** with $n = 14$, 16, and 18. The XRD patterns of the resulting hybrids are shown in Figure 10. Most importantly, the mesostructure obtained from **1(C14)** changed from lamellar to 2D hexagonal, which is ascribed to the decrease of the *g* value. However, **1(C16)** and **1(C18)** formed lamellar structures with thicker siloxane layers, as suggested by the increased *d*-spacings from those of the hybrids prepared without TMOS. It should be noted here that the TMOS-derived species are rarely linked to the cyclic tetrasiloxane species in solution under the conditions we employed. The liquid-state ^{29}Si NMR spectrum of the solution after 2 h of the reaction with TMOS showed the signals of completely hydrolyzed monomer (−71.7 ppm) and dimer (−81.1 ppm) and other oligomeric species, along with those of cyclic tetrasiloxane species derived from **1(C*n*)**. Co-condensation between TMOS- and **1(C*n*)**-derived species probably takes place upon evaporation of the solvent, thereby increasing the headgroup area of alkylsiloxane species.

On the other hand, we examined the use of the oligomer (**2**) having two branched $-Si(OR)_3$ groups, which provide a smaller headgroup than that of **1(C10)**. The liquid-state ^{29}Si NMR spectrum after 12 h of reaction (Supporting Information, Figure S13) mainly shows three signals (−9.1, −12.8, and −20.7 ppm) due to the decylmethylsiloxane unit (D^x, $C_2Si(OSi)_x(OH)_{2-x}$), together with four *Q* signals (−80.0, −80.9, −82.9, and −89.6 ppm). These signals are tentatively assigned to a hydrolyzed oligomer (Q^1−D^2−Q^1), a cyclic trisiloxane (Q^2−D^2−Q^2) formed by intramolecular condensation, and a linear trisiloxane (D^1−

(32) (a) Doshi, D. A.; Gibaud, A.; Goletto, V.; Lu, M.; Gerung, H.; Ocko, B.; Han, S. M.; Brinker, C. J. *J. Am. Chem. Soc.* **2003**, *125*, 11646−11655. (b) Falcaro, P.; Grosso, D.; Amenitsch, H.; Innocenzi, P. *J. Phys. Chem. B* **2004**, *108*, 10942−10948.

(33) (a) Jeffrey, G. A. *Acc. Chem. Res.* **1986**, *19*, 168−173. (b) von Rybinski, W.; Hill, K. *Angew. Chem., Int. Ed. Engl.* **1998**, *37*, 1328−1345.

(34) Israelachvili, J. N.; Mitchell, D. J.; Ninham, B. W. *J. Chem. Soc., Faraday Trans. 1* **1976**, *72*, 1525−1568.

(35) Additional experiments carried out after the submission of this manuscript confirmed that the precursor with $n = 13$ formed a 2D monoclinic structure with $d_{10} = 3.53$ nm (as-synthesized) and 2.93 nm (after calcination).

(36) The lamellar structures were obtained from **1(C14)** and **1(C16)** even when the temperature of the substrate was increased up to 60 °C during the self-assembly, which suggests the strong tendency of these precursors to form a lamellar assembly.

Q^2-Q^1) formed by cleavage of the trisiloxane ring. This precursor solution produced a nanostructured solid that exhibits the XRD peak with $d = 2.92$ nm accompanying the second-order reflection (Supporting Information, Figure S14). Although this d value is very close to that of the **1(C10)**-derived hybrid (Figure 1c), a lamellar structure was confirmed by the collapse of the structure upon calcination. It is likely that the alkyl chains are arranged in a bilayer fashion because the d value is much larger than that expected for an all-trans interdigitated monolayer arrangement.

These results clearly show that the self-assembly of siloxane oligomers with alky chains is governed by their packing parameters, which can be controlled by the number of siloxane units as well as the alkyl chain lengths. It is reasonable to expect that other mesophases that were not observed in the present study can be formed by adjusting the packing parameter of the precursors. In particular, further increase of the headgroup area should lead to the creation of higher curvature mesophases such as 3D hexagonal ($P6_3/mmc$) and cubic ($Pm3n$) phases. The molecular design of new oligomers having more than three $-Si(OR)_3$ groups is underway in our laboratory.

Conclusions

We have demonstrated the formation of silica-based hybrids with ordered mesostructures by self-assembly of designed precursors consisting of oligosiloxane units and alkyl chains of various lengths. The mesostructure of the hybrids, either lamellar or cylindrical assemblies, was controlled by the alkyl chain length and the number of SiO_4 units per alkyl chain. The latter phases could be used to produce porous silica with the pore sizes tunable in the range of micropore (1.1 nm) to mesopore (3.3 nm), which is of great practical interest. These hybrids were mainly formed by the cross-linking of tetrasiloxane rings, generated by the rearrangement of siloxane linkage of the precursors during the reaction. This is in clear contrast to the complicated hydrolysis and polycondensation processes when monomeric alkoxysilanes are used as silica sources. We believe that further modifications of the precursors will allow for the emergence of various hybrid architectures. The use of more rigid and stable siloxane units such as double-four-membered ring (D4R) may lead to the creation of molecularly ordered frameworks. The incorporation of either organic functional groups or other metallic species in the precursors is also very important for a wide range of applications.

Acknowledgment. We are grateful to Mr. D. Mochizuki, Mr. N. Atsumi, and Mr. Y. Yamauchi (Waseda University) for their help in nitrogen adsorption measurement and TEM observation (JEM-2010). We also thank one of the reviewers for many helpful corrections to the original manuscript. The work was partially supported by a Grant-in-Aid for COE Research "Molecular Nano-Engineering", the 21st Century COE Program "Practical Nano-Chemistry", and Encouraging Development Strategic Research Centers Program "Establishment of Consolidated Research Institute for Advanced Science and Medical Care" from MEXT, Japan. A.S. is thankful for financial support from a Grant-in-Aid for JSPS Fellows from MEXT.

Supporting Information Available: Experimental details, spectroscopic data for **1(C*n*)**, Figures S1−S14, and Table S1. This material is available free of charge via the Internet at http://pubs.acs.org.

JA0541736